Astron. Astrophys. 333, 188–198 (1998)

ASTRONOMY AND ASTROPHYSICS

Steps toward interstellar silicate mineralogy

III. The role of aluminium in circumstellar amorphous silicates

H. Mutschke[1], **B. Begemann**[1], **J. Dorschner**[1], **J. Gürtler**[1], **B. Gustafson**[2], **Th. Henning**[1], **and R. Stognienko**[1]

[1] Friedrich-Schiller-Universität Jena, Astrophysikalisches Institut und Universitäts-Sternwarte (AIU), Schillergässchen 2-3, D-07745 Jena, Germany
[2] University of Florida, Astronomy Department, 211 SSRB, Gainesville, FL 32611, USA

Received 21 July 1997 / Accepted 27 November 1997

Abstract. It is a well-known fact that the spectra of oxygen-rich circumstellar dust envelopes around evolved stars show great diversity, especially in the 10 μm silicate band profiles, but also in the longer infrared wavelength range covered by ISO. This supports earlier conclusions that the concept of a universal cosmic silicate is inadequate and that it is reasonable to consider a wider variety of possible silicate analogues as the basis for an improved modelling of the observed spectra. In the course of an investigation of the role of aluminium in cosmic dust, aluminosilicate glasses (ASGs) have been suggested as interesting laboratory analogues for this purpose. In these glasses, silicon ions within the SiO_4 tetrahedra are partly substituted by fourfold coordinated aluminium.

In a new laboratory approach to the silicate dust problem, 13 ASG samples were prepared. Apart from magnesium and iron, the cosmically most abundant metals, sodium and calcium, were incorporated as cations. In this paper, these new silicate dust analogues are analytically and spectroscopically characterized. The spectroscopic results were obtained in the range from the UV to the far-infrared, in the millimetre wave range, and by Raman spectroscopy. Optical constants have been derived for the wavenumbers 1500–20 cm^{-1} (6.7–500 μm) from infrared reflectance measurements and for the frequencies 110–75 GHz (2.7–4 mm) from angle-resolved millimetre-wave scattering at spherical samples from two of the ASGs. For the electronic and vibrational absorption features, the dependence on the aluminium/silicon substitution ratio and on the glass structure is discussed. Relations between the calculated (Rayleigh case) band positions, widths and strengths of the IR absorption bands and the chemical compositions are derived.

The application of the new data to the reproduction of observed stardust spectra of the IRAS-LRS catalogue shows promising results.

Key words: circumstellar matter – stars: AGB and post-AGB – stars: variables: other – infrared: stars

Send offprint requests to: H. Mutschke

1. Introduction

Much experimental work has been done on laboratory analogues in order to understand the cosmic silicate dust (Dorschner & Henning 1986; Krätschmer 1988; Gürtler et al. 1989; Koike & Tsuchiyama 1991; Koike et al. 1993; Jäger et al. 1994 (Paper I); Dorschner et al. 1995 (Paper II)). In Papers I and II silicate glasses with Mg and Fe as the dominant cations and with cation-to-silicon ratios of 1 and 2 were investigated. The approach was based on the following assumptions:

1. The glass state is a good approximation to the structure of the cosmic silicates which are in the amorphous state.
2. Being the most abundant metals in cosmic environments, Mg and Fe are suitable cations for the silicate structure.
3. The stoichiometric ratios are those of olivine and pyroxene, which are common silicates in primitive solar system solids.

The main aim of this experimental simulation was a satisfactory reproduction of the observed profiles of the characteristic vibrational bands at 10 and 19 μm of interstellar and circumstellar silicate dust. Spectra calculated with the help of the laboratory data were compared with the observed silicate spectra of evolved stars (stardust silicates) from the IRAS LRS catalogue (Olnon & Raimond 1986), with the silicate emission of some young stars and the Orion Trapezium nebula, and also with the 10 μm absorption bands of deeply embedded massive young stars. These comparisons have shown that in most cases the band peak positions of the laboratory analogues agree satisfactorily with the observations, whereas the band widths of the laboratory silicates are systematically smaller than those in the observed spectra. As a rule, the "blue wing" of the 10 μm band of the silicate spectra of oxygen-rich envelopes can be reproduced best, whereas the laboratory-based spectra fail to reproduce the width of the 10 μm band, the relatively high absorption observed in the "trough" between the bands, and the extremely flat profile of the 20 μm band.

A study of aluminium oxide in the context of the explanation of the 13 μm band in oxygen-rich stars (Begemann et. al. 1997) turned our attention to the role of aluminium in circumstellar solids. If Al_2O_3 should condense in these envelopes, its incorpo-

ration into circumstellar silicates cannot be excluded. Environments where aluminium condensation might play a significant role in the evolution of the dust have been discussed previously (Stencel et al. 1990). The possible significance of this element is also suggested by the role of Al in the high-temperature silicates in the so-called CAI (calcium aluminium inclusions) in primitive meteorites (MacPherson et al. 1988). Among the metals, aluminium holds the fourth position after Si, Mg, and Fe in the table of elemental abundances (Palme & Beer 1993). In a basic paper on circumstellar grain formation and metamorphism, Nuth (1996) considers amorphous oxides of the type MeO_x (with Me standing for Si, Mg, Fe, and Al) as primary nucleation products, from which silicates are formed. Besides stardust silicates, there are indications that aluminium may also be expected in silicates condensed out of the interstellar gas because Al is strongly depleted in the gas phase (Whittet 1992). On the other hand, GEMS (glasses with embedded metal and sulfide) which are contained in interplanetary dust grains and have been supposed to represent interstellar silicates show Al/Mg atom number ratios up to 0.46 (Bradley & Ireland 1996). The average solar system ratio amounts to 0.08.

The striking variations of the stardust silicate features from source to source (see, e.g., Sloan & Price 1995 and literature cited therein) and the indications of crystalline admixtures to the silicate dust found in ISO SWS spectra of oxygen-rich dust shells (Waters et al. 1996) encourage study of a greater chemical and structural variety in the laboratory analogues (cf. Dorschner 1997). This observational evidence and the aforementioned arguments in favour of a greater significance of aluminium in dust chemistry led us to prepare four series of aluminosilicate glasses (ASGs). Here we should note that glasses already represent an amorphous state with a well-developed short-range order, which might not be typical of the very primary silicatic stardust condensates. The latter could be less ordered and not fully oxidized like the "chaotic silicates" proposed by Nuth & Hecht (1990).

Mineralogically aluminosilicates are characterized by a partial substitution of the fourfold coordinated silicon atoms by aluminium. Since aluminium is only trivalent, compensation for the negative charge excess of the AlO_4-tetrahedra requires the addition of mono- and/or divalent cations. In terms of glass structure, Al together with Si acts as the network former in ASGs. The objective of our work was to study the influence of the substitution ratio Al/(Si+Al) on the infrared spectra. For maintaining the charge balance we used the metal cations Mg^{2+}, Mg^{2+}/Fe^{2+} (mixed), Na^{+} and Ca^{2+}. Except for calcium, we prepared series of samples with systematically varying Al content. Metal/Al ratios of at least 1 for the monovalent and at least 0.5 for the divalent metal ions are required for charge balance.

Apart from the charge-balancing function, however, the metal ions also act as network modifiers, i.e., they break the polymerization of the $(Si/Al)O_4$-tetrahedra. Therefore, another very important structural parameter is the degree of polymerization which is expressed in this paper by the number of non-bridging oxygen atoms per tetrahedron ($\mathrm{NBO/T} = 20/(\mathrm{Si} + \mathrm{Al}) - 4$). Within each series, we tried to keep NBO/T approximately constant in order to produce similar silicate structures. For the Mg- and Mg/Fe-ASG series, which structurally resemble the formerly studied pyroxene glasses (NBO/T≈2, see Paper II), this is done by means of a constant metal content with respect to silicon. The structure of the Na series differs strongly from these because it resembles tectosilicates (NBO/T=0). In the case of these silicates, the small amount of Na is incorporated into the spatial silicate network without changing it drastically (see Sect. 3). The compositions of the Ca-ASGs are similar to the minerals gehlenite and melilite as well as to anorthite, the Ca endmember of the plagioclas series. These highly refractory minerals are major components of the CAIs (calcium aluminium inclusions).

In this paper we present the experimental results, make available the optical constants of the ASG series, and point to some astrophysical applications to the stardust mineralogy. In Sect. 2 the preparational steps and basic analytical results are described, including a Raman-spectroscopical investigation of the role of aluminium in the glass structure. Sect. 3 reports infrared reflectance measurements, from which optical constants in the wavelength range 6.7–500 μm have been derived, and the determination of refractive indices from millimetre-wave scattering measurements. In Sect. 4 the results are discussed and applied to the reproduction of the dust spectra of oxygen-rich circumstellar envelopes.

2. Preparation and analytics

2.1. Preparation of ASG series

The sum formulae of the prepared ASGs are given in Table 1. The parent substances of the melts were sodium carbonate, magnesium carbonate, ferrous oxalate, calcium carbonate, aluminium oxide and silicon dioxide. Aluminium oxide was freshly prepared each time by heating aluminium hydroxide in air at 1273 K for 1 hour. Each mixture was placed in a platinum-rhodium crucible and slowly heated in a resistance furnace in air to a temperature between 1823 K and 1923 K, which was maintained for 1 hour. In some cases, the maximum furnace temperature of 1973 K limited the compositional range in which melting of the mixture was possible.

The Mg-, Mg-Fe-, and Ca-ASG melts were quenched by pouring them through rotating copper rollers. By this method, amorphous slabs of about 0.1 mm thickness were formed. In the case of the sodium aluminosilicates, this method failed because of the high viscosity of the melts. Fortunately, quenching under flowing water was sufficient to obtain a glassy material. However, the high viscosity prevented the carbon dioxide (formed by the decomposition of sodium carbonate) from leaving the hot melts, which led to a large number of bubbles in the glasses. In order to reduce the number of bubbles, the Na-ASGs were powdered and melted a second time. After the second quenching the number of bubbles was small, and pieces of glass up to 1 cm in diameter could be broken out of the crucible content.

Table 1. Structural and chemical parameters of the ASG samples. The formulae in brackets denote the weight fraction of the substance. The iron oxide fraction contains both ferrous and ferric iron.

Sum Formula (theor.)	Al/(Al+Si) (theor.)	NBO/T (theor.)	Density (g cm^{-3})	[Na_2O]	[MgO]	[Fe_2O_3]	[CaO]	[Al_2O_3]	[SiO_2]
				(wt %)					
$NaAlSi_2O_6$	0.33	0	2.40	13.6				24.7	58.8
$NaAlSi_3O_8$	0.25	0	2.36	10.8				19.1	68.1
$NaAlSi_4O_{10}$	0.20	0	2.30	8.5				15.4	73.3
$Mg_2AlSi_2O_{7.5}$	0.33	1	2.82		32.5			19.2	47.4
$Mg_3AlSi_3O_{10.5}$	0.25	1.25	2.93		34.9			14.0	49.3
$Mg_4AlSi_4O_{13.5}$	0.20	1.4	2.90		36.5			11.1	52.4
$Mg_9AlSi_9O_{28.5}$	0.10	1.7	2.81		38.7			6.3	55.9
$MgFeAlSi_2O_{7.5}$	0.33	1	3.10		14.6	26.5		17.0	42.1
$Mg_{1.5}Fe_{1.5}AlSi_3O_{10.5}$	0.25	1.25	3.10		14.6	28.5		12.7	43.9
$Mg_2Fe_2AlSi_4O_{13.5}$	0.20	1.4	3.16		16.0	29.7		9.1	45.7
$Mg_{4.5}Fe_{4.5}AlSi_9O_{28.5}$	0.10	1.7	3.16		16.6	31.2		4.6	48.1
$Ca_2Al_2SiO_7$	0.67	0.67	2.91				40.5	36.5	22.1
$Ca_2Mg_{0.5}AlSi_{1.5}O_7$	0.40	1.6	3.03		10.0		37.3	17.9	34.1

2.2. Analytical characterization

The glass samples were embedded into epoxide resin and polished in order to prepare them for IR reflectance spectroscopy. A part of the quenched glasses was powdered for wet-chemical analysis and X-ray diffraction. Expectedly the X-ray diffractograms did not show any Bragg reflexes in the angular range of 2θ from 10 to 60°. By scanning electron microscopy investigation, the homogeneity of the glasses was confirmed. No phase separations could be seen up to a magnification of 20 000.

The powdered samples left for wet-chemical analysis (500 mg) were fused with anhydrous soda and borax, and the resulting melts were dissolved in hydrochloric acid. The SiO_2 content of the solutions was determined after precipitation with polyethylene oxide by gravimetric analysis. In the remaining solution the content of calcium, magnesium, iron, and aluminium oxides was successively determined by complexometric titration. The sodium oxide content of the glasses was determined by an additional digestion. After the decomposition of 500 mg of the powdered glass by hydrofluoric acid and sulphuric acid, aluminium and silicon were precipitated with calcium hydroxide. The sodium ions remained in the solution and were subsequently precipitated as sodium sulphate (Lange 1991). The composition of the glasses in terms of weight fractions of the oxides are listed in Table 1. Deviations of our results from the theoretical composition are mainly due to evaporation losses during the melting process. This especially happened to the sodium and calcium where the deviations are of the order of 10% of the theoretical value. Magnesium is enriched in the Ca-ASG by about 30%. In all other cases the deviations are small.

The density of the glasses has been determined both by Archimedes' method in ethanol and by means of a He-pycnometer. The latter values are systematically larger by about 5 % because He can penetrate into smaller pores than ethanol. The density depends on the cations and on the SiO_2 content. The latter dependence is clearly indicated in the Na-ASG series.

2.3. Raman spectroscopy

Raman spectroscopy has been used to check the degree of polymerization of the glasses. The spectrum of a highly polymerized three-dimensional network like quartz glass is expected to be characterized by strong bands in the range around 500 cm^{-1}, which are due to vibrations involving the bridging oxygens, and by only weak bands in the Si–O stretching region at 900-1200 cm^{-1} (Mysen et al. 1980). When network modifiers that create non-bridging oxygens are introduced, the strength of the stretching bands increases compared to the 400-800 cm^{-1} band group and new stretching band components appear in the 800–1000 cm^{-1} region. For instance, McMillan (1984) has shown for alkaline-earth silicate glasses, that the Si–O stretching band group can be deconvoluted into four bands which are assigned to symmetric vibrations of the silicate tetrahedra with one, two, three, and four non-bridging oxygen atoms.

We measured the Raman spectra at polished surfaces of the ASGs by means of a Raman microscope (LABRAM 1, Dilor), using the 632.8 nm line of a HeNe laser with a power of 15 mW for excitation. The spectra have been recorded from 200 to 1500 cm^{-1} Raman shift, and have been deconvoluted into individual bands with Gaussian profiles (see Table 2). For our Na-ASGs we found in accordance with the results by Mysen et al. (1980,1981) and Sharma et al. (1979) that the Raman spectra are similar to those of glassy SiO_2. This points to a three-dimensional network of SiO_4- and AlO_4-tetrahedra and confirms that aluminium indeed acts as a network former. With increasing aluminium content the bands shift towards lower wavenumbers due to the smaller force constants of the Al–O bonds compared with Si–O bonds.

For the Mg- and Mg-Fe-ASGs the stretching band group is stronger and centres at lower wavenumbers compared with the sodium glasses. The opposite is true for the low-wavenumber band group. This behaviour reflects the presence of non-bridging oxygens introduced by network modifier cations. How-

Table 2. Raman bands of ASGs in comparison to SiO_2 glass. Abbreviations: s strong; m medium; w weak. The estimated wavenumber uncertainty is about ± 10 cm^{-1}.

formula	wavenumber (cm^{-1})							
SiO_2	430s	483s	595w	790m			1059w	1188m
$NaAlSi_4O_{10}$	390s	477s	586m	797w			1006w	1124m
$NaAlSi_3O_8$	411s	483s	585m	793w			995w	1105m
$NaAlSi_2O_6$	414s	486s	579m	767w			970w	1063m
$Mg_2AlSi_2O_{7.5}$			589w	717w	871w	910m	966s	1024w
$Mg_3AlSi_3O_{10.5}$			595w	704w	876w	911m	973s	1023w
$Mg_4AlSi_4O_{13.5}$			603w	710w	878m	919m	976s	1031w
$Mg_9AlSi_9O_{28.5}$			614w	691m	880w	907m	972s	1026w
$MgFeAlSi_2O_{7.5}$		492s	581s	692s	866w	903m	953m	1010m
$Mg_{1.5}Fe_{1.5}AlSi_3O_{10.5}$		524s	588m	702m	863w	906m	969s	1025m
$Mg_2Fe_2AlSi_4O_{13.5}$		538s	583m	704m	876w	918m	979s	1049m
$Mg_{4.5}Fe_{4.5}AlSi_9O_{28.5}$		515m	587m	696m	865w	912m	978s	1048m
$Ca_2Al_2SiO_7$		532m	560s	651w	872m	900s	975m	1036w
$Ca_2Mg_{0.5}AlSi_{1.5}O_7$			574m	693w	866s	917s	994m	1039m

ever, this decrease of polymerization seems to be less significant in the Mg-Fe-ASGs than in the Mg-ASGs. The reason is probably the formation of additional tetrahedra by Fe^{3+} ions. An oxidation of a considerable part of the Fe^{2+} to Fe^{3+} during the melting process is indeed likely. In this case, the magnesium charge-balances both the Fe^{3+} and the Al^{3+} in the tetrahedra. As the result, the NBO/T could decrease down to much smaller values than those given in Table 1.

The polymerization increases with increasing aluminium content, which is reflected by a growing intensity of the low-wavenumber band group and by the high viscosity of the aluminosilicate melts. The theoretical sum formulae $Ca_2Mg_{0.5}AlSi_{1.5}O_7$ and $Ca_2Al_2SiO_7$ give a NBO/T ratio of about 1.6 and 0.67, respectively. Therefore, it is not surprising that the Raman spectra of $Ca_2Mg_{0.5}AlSi_{1.5}O_7$ resemble those of the Mg-ASGs, whereas the Raman spectra of $Ca_2Al_2SiO_7$ are similar to those of the Mg-Fe-ASGs.

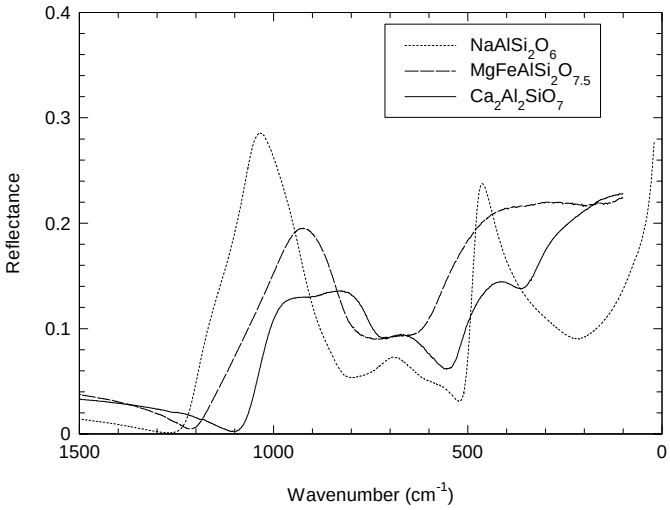

Fig. 1. Typical reflectance spectra of three of the aluminosilicate glasses. See text for the discussion.

3. Derivation of optical constants

3.1. UV/VIS/NIR spectroscopy

In order to determine the optical properties of the ASG materials, we studied the reflectance of polished samples embedded in resin from the UV to the FIR (0.2–500 μm), the transmittance of the original thin slabs in the transparent region in the visible and near-infrared (VIS/NIR) and, for two materials, the scattering of millimetre-sized spheres in the millimetre-wave region.

It turned out that the spectral behaviour of the Mg- and Ca-ASG samples in the UV/VIS/NIR range is similar to that of the Mg-pyroxene glass studied in Paper II. The materials are completely transparent in the visible, and the fundamental electronic UV absorption starts at about 350 nm (for $\approx$0.1 mm thick slabs) independent of the Al content. This is not surprising because the UV edge is caused by the non-bridging oxygen atoms which are abundant in the structures of these materials. In contrast to this, the Na-ASG samples are expected to be more transparent in the UV because NBO/T$\approx$0. Unfortunately, a UV measurement of these samples was not possible because of their porosity. The shape of the UV/VIS/NIR spectra of the Mg-Fe-ASG samples is determined by the iron ions. As in the case of Mg-ASGs, good qualitative and quantitative agreement with the $Mg_{0.5}Fe_{0.5}SiO_3$ glass studied in Paper II was found, independent of the aluminium content.

Since the study of the UV/VIS/NIR region obviously does not provide any significant new information in addition to that gained from the study of the pyroxene glasses in Paper II, we restrict the discussion of the optical properties of the ASGs in the following to the MIR, FIR, and millimetre regions.

3.2. Infrared spectroscopy

The infrared reflectance measurements have been carried out at near-normal incidence using a Bruker 113v FTIR spectrometer.

The examples shown in Fig. 1 give an impression of the variability of the infrared spectra of the materials that have been studied here. Differences are seen not only in the shapes of the main silicate features at about 10 and 20 μm, but also in the trough between them and in the far-infrared.

The spectrum of the Na-ASG appears similar to that of quartz glass (SiO_2), though the 10 μm (corresponds to 1000 cm^{-1}) and 20 μm bands (500 cm^{-1}) of the latter are stronger (cf. Henning & Mutschke 1997). The 10 μm band is assigned to Si(Al)–O stretching vibrations and the 20 μm band to the bending vibrations of bridging oxygens perpendicular to the Si(Al)–O–Si(Al) plane. In the trough region between these bands, there is a feature which in SiO_2 is assigned to in-plane bending vibrations of the Si–O–Si linkages. A significant difference of the Na-ASG spectrum is the rise of the reflectivity in the far infrared, which is due to vibrations of the sodium ions relative to the SiO_4 tetrahedra. These localized vibrational modes of the network-modifier ions have been studied in detail by Gervais et al. (1987). In the Ca-ASG spectrum the corresponding vibrations of the calcium ions are observed as a rise in reflectivity at about 300 cm^{-1}. For Mg- and Mg-Fe-ASGs, the metal vibrations occur close to the frequency of the 20 μm band and cause a significant broadening of this band (Gervais et al. 1987).

The IR spectrum of the Mg-Fe-ASG is similar to those of the previously studied pyroxene glasses (cf. Paper II). Compared to the Na-ASG, the 10 μm feature is shifted to longer wavelengths, which is explained by the weaker polymerization of the silicate network (NBO/T=1...1.7). The trough region does not show any feature but is less deep than in the Na-ASG spectrum. The Ca-ASG is the Al-richest sample. In fact, this glass contains two times more aluminium than silicon. Its spectrum shows a very strong red-shift and a splitting of the 10 μm feature. The red-shift in this case probably is not only due to the degree of polymerization of the network because NBO/T is relatively low (see Table 1). Therefore, the substitution of silicon by aluminium should play an important role for the shift. The splitting probably indicates the presence of differently polymerized tetrahedra (see McMillan 1984 for silicates) though according to Gervais et al. (1987) the tendency of Ca to cause band splitting is low. A band splitting due to Al/Si substitution has not yet been mentioned in the literature, but, to our knowledge, such high substitution ratios have not been studied so far. In the trough there is again a feature, the position of which is comparable to that of the Na-ASG trough band.

Unfortunately, we were not able to measure useful FIR reflectance spectra below 100 cm^{-1} for those silicate glasses which have been quenched by means of the copper rollers. As described in Paper II, interferences due to multiple reflection occur in the reflectance spectra of these samples. Due to the polishing process the thickness of the glass slabs is inhomogeneous. Therefore, the spectrum cannot be modelled in this wavelength region and this part of the spectrum has been discarded.

From the reflectance spectra, the complex refractive index $m = n + ik$ of the materials has been calculated by means of the Kramers-Kronig analysis described already in Paper II. For the roller-quenched samples, the reflectance was set constant for wavenumbers smaller than 100 cm^{-1} and for the Na-ASGs for wavenumbers smaller than 20 cm^{-1}. The resulting wavelength dependence of n and k is shown in Fig. 2. [1]

The k-spectra show more clearly than the reflectance spectra the structure of the vibrational transitions in the glasses, for instance of the metal-ion localized modes in the FIR (Na: $<$100 cm^{-1}, Ca: 250 cm^{-1}, Mg: 400 cm^{-1}, Mg/Fe: 300 cm^{-1}). It is interesting that for the aluminium-poor Mg- and Mg-Fe-ASG samples, these features are well separated from the silicate bending mode whereas for the aluminium-rich glasses the separation vanishes. This effect is probably caused by a shift of the bending modes due to increasing polymerization (see NBO/T in Table 1). Another possibility could be a shift because of the increasing proportion of AlO_4-tetrahedra which could have another bending-mode frequency. However, no shift is found with the Na-ASGs where the substitution ratio changes but not the degree of polymerization. This strongly supports the first explanation.

In all series the 10 μm stretching band is shifted towards lower wavenumbers with increasing aluminium content. Except for the $Ca_2Al_2SiO_7$ glass, no splitting of the 10 μm band is observed. This is consistent with the results of Gervais et al. (1987) from a limited range of ASG compositions. Obviously, the comparable masses and ionic radii of Si and Al result in very similar resonance frequencies for the stretching vibrations of AlO_4 (lower frequency) and SiO_4 tetrahedra. Consequently, the vibrations are allowed to couple by long-range Coulombic interaction and appear as a single absorption band. The shift of the band reflects, thus, the varying abundance ratio of the two types of tetrahedra.

The trough region is especially interesting because aluminium oxide vibrations occur in this spectral range. For Na-ASGs, there is an interesting shift of the already mentioned trough band from about 800 cm^{-1} to 700 cm^{-1}. This shift has been observed also by Gervais et al. (1987), who attributed it to a frequency shift of the in-plane bending vibrations well known from SiO_2. In our spectra, however, two bands are clearly resolved in the spectra of low-Al samples so that the alternative interpretation by Tarte (1965) in terms of a localized mode seems more adequate than that by the coupled AlO_4/SiO_4 vibration. For substitution ratios larger than about 0.25 (see also the Ca-ASGs), the 700 cm^{-1} band is clearly dominant and is not shifted further.

In the Mg- and Mg-Fe-ASGs there is no distinct trough band but a relatively flat trough bottom which rises considerably with increasing aluminium content. This filling of the trough must be due to the increase of an additional band. A weak indication of a maximum at about 700 cm^{-1} in the Al-richest spectra indeed points to the vibrational mode already observed in Na- and Ca-ASGs.

[1] The n- and k-data files of all ASG samples can be taken from the internet homepage of the Astrophysical Institute and University Observatory Jena (http://www.astro.uni-jena.de).

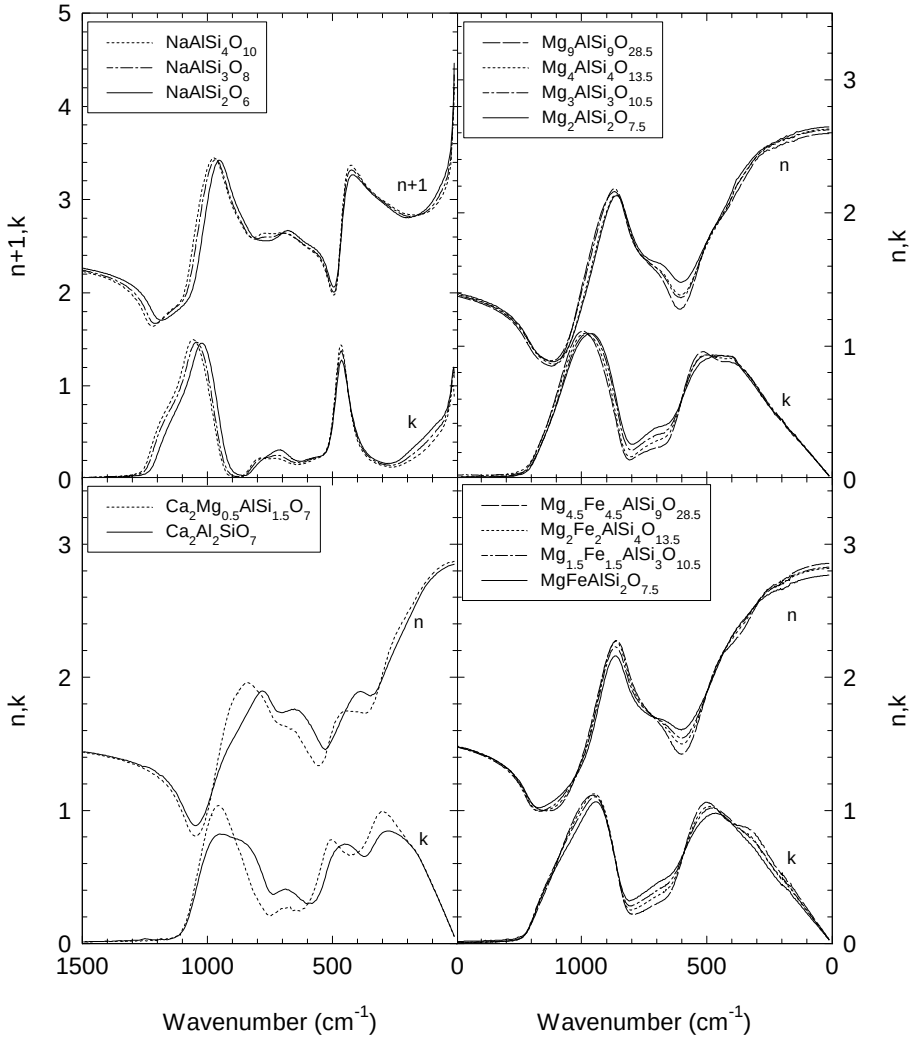

Fig. 2. Optical data calculated by Kramers-Kronig analysis of the reflectance spectra of aluminosilicate glasses.

Table 3. Optical data in the millimetre range determined by angle-resolved scattering measurements on spheres and calculated mass absorption coefficient κ_m(110 GHz) for spheres in the Rayleigh limit

Formula	Mass	d (fitted)	Complex refractive index $n+ik$ at frequency (GHz):					κ_m(110 GHz)
	(g)	(mm)	75	80	90	100	110	cm^2g^{-1}
$Mg_2AlSi_2O_{7.5}$	0.278	5.88	2.70+0.04i				2.71+0.055i	0.184
$Mg_2AlSi_2O_{7.5}$	0.645	7.61	2.70+0.03i				2.70+0.03i	0.101
$MgFeAlSi_2O_{7.5}$	0.360	6.08	2.87+0.05i	2.86+0.06i	2.86+0.04i	2.85+0.05i	2.85+0.04i	0.109

3.3. Millimetre-wave measurements

For the two Al-richest Mg- and Mg-Fe-ASG materials, the optical data n and k in the millimetre region have been determined by a scattering experiment. For this purpose, spheres of about 6–8 mm diameter were produced from glass pieces obtained by quenching the melts in water. The setup of the angle-resolved scattering experiment carried out at frequencies between 75 GHz (wavelength 4 mm) and 110 GHz (2.73 mm) is described elsewhere (Gustafson 1996). The scattered intensities have been recorded in an angular range from 0° to 165° with a resolution of 0.1°. The scattering curves have been fitted by Mie theory in order to obtain the n- and k-values (Table 3). They do not show significant dependence on the frequency in this range. The n-values match very well the extrapolation of the n-spectra in Fig. 2. The k-values indicate that the slope of the absorbance is less steep in the millimeter range than an extrapolation of the FIR slope would suggest (see Fig. 4). This is consistent with previous studies of the low-frequency optical properties of glasses. Bösch (1978), e.g., reports increased (anomalous) absorption for a silica-lime glass at millimetre wavelengths, which is attributed to tunneling processes in the glass structure. The mass absorption coefficients calculated from these optical data (see Table 3) may be compared with the compilation of opacity values at 1 mm wavelength given by Henning (1996).

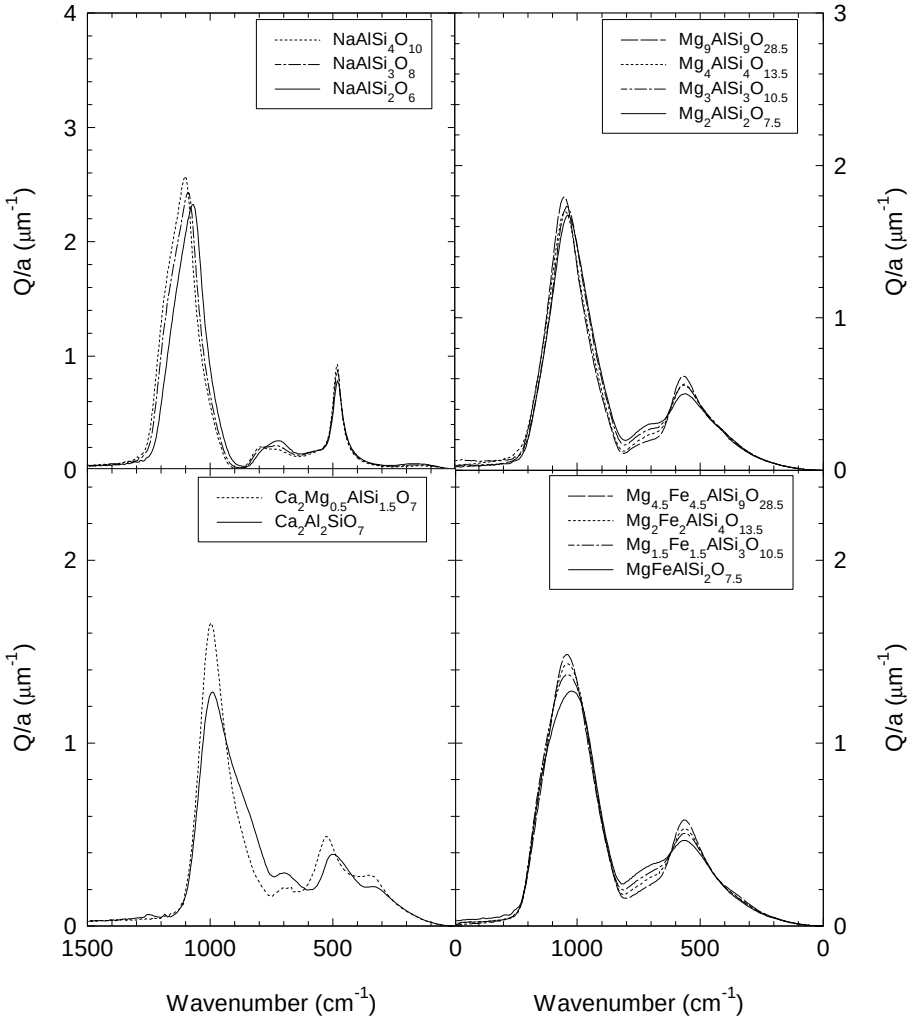

Fig. 3. Absorption spectra for spherical grains small compared to the infrared wavelengths (Rayleigh limit) in vacuum. The spectra have been calculated from the optical data of Fig. 2. Q is the efficiency factor for absorption of a spherical grain with radius a.

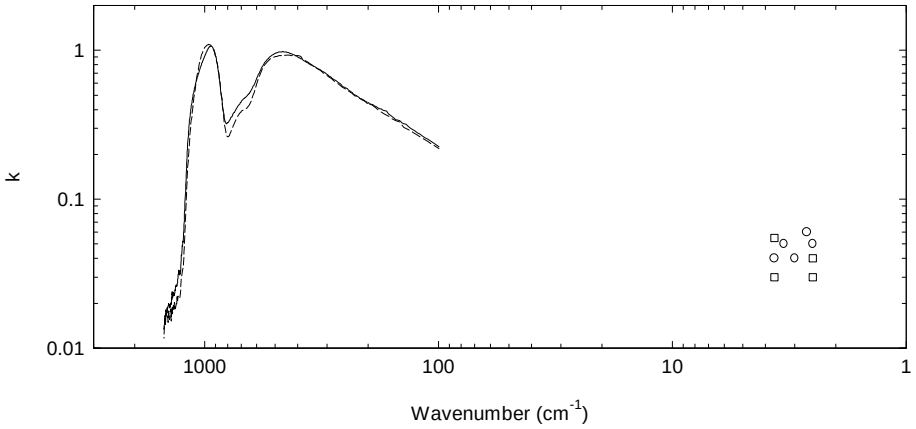

Fig. 4. Absorption indices determined from millimetre-wave scattering compared to those of Fig. 2 for the samples $Mg_2AlSi_2O_{7.5}$ (squares and dashed line) and $MgFeAlSi_2O_{7.5}$ (circles, solid line).

4. Discussion

4.1. Diagnostic relations

At first sight the IR spectra of many silicate glasses appear similar. Statistical fluctuations of the lengths and the angles of the Si–O bonds of the tetrahedra that form the glass network cause this similar appearance of the profiles. However, thorough examination of the spectra reveals differences in the band positions, widths, strengths, and, in particular, in the shape of the trough, the region between the main bands. In Paper II, we called those characteristics that depend on the chemical composition of the glasses "diagnostic parameters" because they may help with the identification of the cosmic silicates.

Fig. 3 shows the wavelength dependence of the emissivity of spherical grains from the various substances studied in this paper in terms of Q/a, where Q is the efficiency factor of

Table 4. Diagnostic parameters of the characteristic bands of the ASGs taken from small spheres within the Rayleigh limit (Fig. 3). The meaning of the symbols is as follows: λ peak position of a band, $S = Q/a$ absorption coefficient, W full width at half maximum of a band, $B = S(20)/S(10)$ band ratio, $T = S_{\min}(\mathrm{trough})/S(10)$ trough ratio, * no evaluation possible, ** shoulder at about 14 μm. In addition to the Mg-ASG and the Mg-Fe-ASG series, the data of the pyroxene glasses are given for the sake of comparison

Formula parameter	10 μm band			20 μm band			13 μm band	band ratio	trough ratio
x	$\lambda(10)$ (μm)	$S(10)$ ($\mu\mathrm{m}^{-1}$)	$W(10)$ (μm)	$\lambda(20)$ (μm)	$S(20)$ ($\mu\mathrm{m}^{-1}$)	$W(20)$ (μm)	$\lambda(13)$ (μm)	B	T
$NaAlSi_xO_{2x+2}$:									
x=2	9.36	2.33	1.26	20.8	0.78	2.3	13.9	0.33	0.01
3	9.19	2.43	1.24	20.8	0.87	2.1	13.3	0.36	0.01
4	9.08	2.57	1.19	20.8	0.92	2.0	12.6	0.36	0.01
$Mg_xAlSi_xO_{3x+1.5}$:									
x=2	9.65	1.67	1.92	17.8	0.50	11.5	**	0.30	0.12
3	9.61	1.73	1.80	17.7	0.56	9.0	**	0.32	0.10
4	9.53	1.70	1.77	17.7	0.57	8.0	**	0.34	0.07
9	9.48	1.79	1.63	17.6	0.62	6.6	**	0.35	0.06
$MgSiO_3$:	9.32	1.72	1.64	17.7	0.66	5.95	–	0.38	0.08
$Mg_{0.5x}Fe_{0.5x}AlSi_xO_{3x+1.5}$:									
x=2	9.80	1.28	2.48	17.8	0.47	11.7	**	0.37	0.18
3	9.62	1.37	2.36	17.8	0.50	10.1	**	0.37	0.14
4	9.63	1.43	2.26	17.8	0.53	8.7	**	0.37	0.12
9	9.60	1.48	2.12	17.8	0.58	7.0	**	0.39	0.10
$Mg_{0.5}Fe_{0.5}SiO_3$:	9.25	1.32	2.27	17.9	0.57	6.64	–	0.44	0.12
$Ca_2Mg_{0.5}AlSi_{1.5}O_7$:	10.04	1.66	1.35	19.1	0.49	*	14.5	0.29	0.10
$Ca_2Al_2SiO_7$:	10.10	1.28	2.32	20.0	0.39	*	14.1	0.30	0.15

absorption and a the grain radius. The mass absorption coefficient κ_m follows by multiplication of Q/a with $3/(4\delta)$ with the density δ from Table 1. The efficiency factors were computed by means of Mie's theory for small spherical grains (Rayleigh limit) in vacuum and then used to derive the numerical values of the diagnostic parameters. The resulting values for the ASGs studied in this paper are listed in Table 4. For the sake of comparison, we added the values of the diagnostic parameters of the pyroxene glasses $MgSiO_3$ and $Mg_{0.5}Fe_{0.5}SiO_3$ from Paper II.

The diagnostic parameters of the ASGs are tightly correlated with chemical parameters. In Table 5 the results of the linear regression of the spectral characteristics with the SiO_2 and the Al_2O_3 content are given. In most cases the correlation coefficient is larger than 0.9. The coefficients in the relations of $\lambda(10)$ and $W(10)$ with the SiO_2-content for the Mg- and Mg-Fe-ASGs agree with the results of Koike & Hasegawa (1987).

As the values listed in Table 4 show, the band properties of the Mg-ASG and the Mg-Fe-ASG series are very similar to those of the pyroxene glasses $MgSiO_3$ and $Mg_{0.5}Fe_{0.5}SiO_3$, respectively. However, the latter in some parameters do not fit exactly into the trend established by the former. Especially, band strengths and widths of the 10 μm bands and also the trough ratios of the pyroxene glasses correspond to those of ASGs richer in Al. In contrast to this, the 10 μm band positions and the band ratios of the pyroxene glasses are rather extreme compared to the ASGs. These differences may indicate a slightly different glass structure.

The strengths and widths of the 20μm band show a strong dependence on the Al content. Their values also nearly perfectly converge towards those of the Al-free pyroxene glasses. The particularly large variation of $W(20)$ with the Al content is, however, strongly influenced by the increase of the trough level which merges with the band.

The profiles of the main silicate bands of the Na-ASGs are considerably different from those observed in astronomical sources. Therefore, these glasses are not astrophysically important. The Ca-ASGs are, however, particularly interesting because they combine significant trough absorption with rather flat 20 μm band profiles. If Ca-ASGs play a significant role in stardust grains they should contribute to filling up the trough and

Table 5. Regression analysis of the relations between the spectral (Y) and the chemical parameters (X) of the aluminosilicate glasses. The relations are of the type $Y = a + 0.01bX$, where X is either [SiO_2] or [Al_2O_3], and r is the correlation coefficient. The meaning of the symbols is as follows: λ peak wavelengths of the 10-, 20-, and 13-μm bands, $S = Q/a$ band strengths, W FWHM of the bands, [SiO_2] and [Al_2O_3] contents of SiO_2 and Al_2O_3, respectively. The quantities are given in the same units as in Tables 1, 4

Spectral parameter	[SiO_2] a	b	r	[Al_2O_3] a	b	r
Na-ASGs						
$\lambda(10)$	10.5	-1.92	-1.00	8.62	3.01	1.00
$\lambda(13)$	19.1	-8.73	-0.99	10.5	13.8	0.99
$S(10)$	1.38	1.59	0.97	2.94	-2.51	-0.98
$W(10)$	1.53	-0.45	-0.92	1.09	0.72	0.94
Mg-ASGs						
$\lambda(10)$	10.6	-2.04	-0.99	9.39	1.38	0.97
$\lambda(20)$	18.7	-2.04	-0.93	17.5	1.48	0.98
$S(10)$	1.03	1.39	0.90	1.83	-0.83	-0.88
$S(20)$	-0.08	1.25	0.95	0.68	-0.90	-0.99
$W(10)$	3.37	-3.09	-0.97	1.50	2.19	0.99
$W(20)$	35.8	-52.8	-0.95	3.98	37.9	0.99
Mg-Fe-ASGs						
$\lambda(10)$	11.0	-2.88	-0.80	9.50	1.46	0.83
$\lambda(20)$	–	–	–	–	–	–
$S(10)$	-0.09	3.29	0.98	1.56	-1.61	-0.99
$S(20)$	-0.30	1.83	1.00	0.62	-0.88	-0.99
$W(10)$	4.98	-5.95	-1.00	1.99	2.89	1.00
$W(20)$	44.4	-78.0	-1.00	5.25	38.0	1.00

to flattening the 20 μm band. Both effects are desirable in order to make the laboratory-based spectra more compatible with the observed ones.

4.2. Astrophysical application to stardust silicates

From the viewpoint of the mean cosmic elemental abundance, the Mg- and Mg-Fe-ASGs deserve the greatest attention in any astrophysical context. Aluminium is about a factor of ten less abundant than these elements. The role of other elements as ingredients of silicates is not yet so clear. Since the mean cosmic elemental abundance is tantamount to the chemical composition of the solar photosphere and the chondrites, the basic question is how representative this mean cosmic abundance is for the expanding atmospheres of oxygen-rich evolved stars where the silicate grains are formed. If the identification of the 13 μm band observed in many spectra of such stars with Al_2O_3 is correct, then we have conclusive evidence that Al plays a role in circumstellar dust mineralogy. However, if Al is important, then both sodium and calcium must not be neglected since their abundance is only slightly less than that of Al (Palme & Beer 1993).

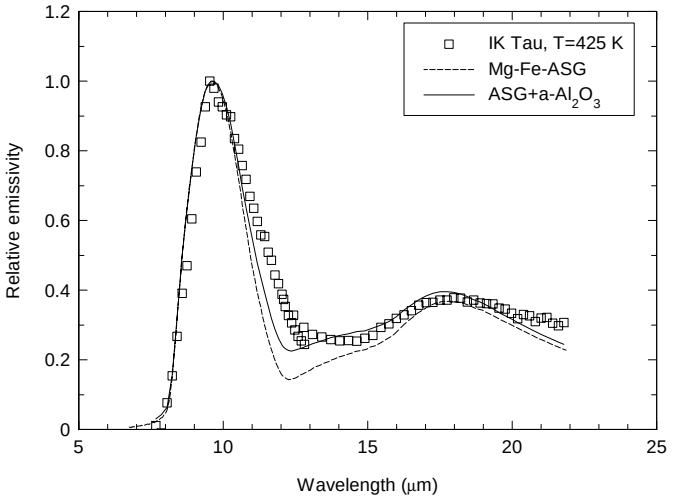

Fig. 5. Normalized IR absorption coefficient derived from the IRAS LRS of the star IK Tauri (squares). The dust temperature was assumed to 425 K. The dashed line is the normalized absorption coefficient (Rayleigh case) of the $Mg_{1.5}Fe_{1.5}AlSi_3O_{10.5}$ glass. The solid line shows the change of the calculated absorption spectrum by the addition of 10 vol.% a-Al_2O_3.

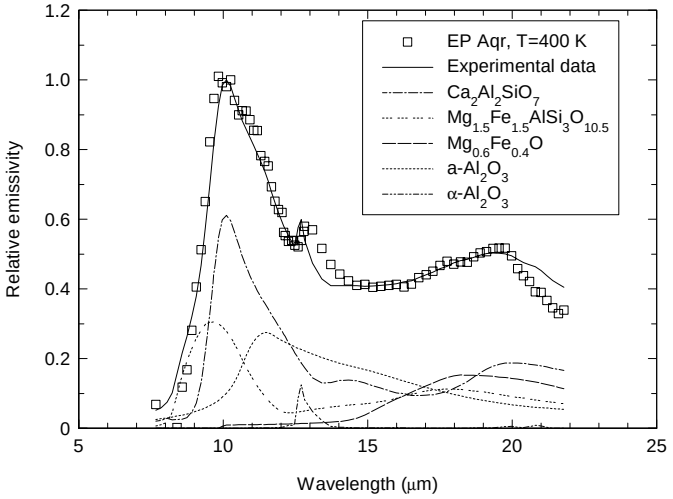

Fig. 6. IR absorption coefficient derived from the IRAS LRS of the star EP Aquarii (squares). The dust temperature was assumed to amount to 400 K. The solid line is a synthetic spectrum obtained by a combination of the absorption coefficients of $Ca_2Al_2SiO_7$ with Mg-Fe-ASG (x=3), amorphous and crystalline Al_2O_3, and $Fe_{0.4}Mg_{0.6}O$.

Quite another question is to understand the formation of such grains. Ca and Na have nearly the same cosmic abundance, but their compounds must form in different thermal conditions in cosmic environments. In the CAI, Ca-bearing components dominate over Na compounds (MacPherson et al. 1988). However, the CAI components anorthite and melilite which are compositionally related to our Ca-ASGs, are crystalline minerals. Generally, the CAI are probably secondary modification products rather than primary condensates of the solar nebula (MacPherson et al. 1988).

In Figs. 5 and 6 we compare absorption spectra calculated for Rayleigh spheres from our laboratory data with the absorption coefficients derived from IRAS LRS spectra of two oxygen-rich evolved stars. The silicate spectrum of IK Tauri is characterized by a narrow 10 μm band peaking at 9.6 μm, a flat trough, and a symmetric 20 μm band with its peak at 18.2 μm. The spectrum of the second star, EP Aquarii, shows a broader 10 μm band peaking at 10.0 μm, a relatively strong 13 μm band, excessive trough absorption, and an asymmetric 20 μm band with its peak around 19.6 μm. Fig. 5 shows that the Mg-Fe-ASG for x=3 gives a satisfactory representation of the blue wing and the relatively sharp peak of the 10 μm band of the Mira-star IK Tau. Also, the 20 μm band is well matched. In the trough region, the level of absorption is not yet sufficient. This can be considerably improved by adding grains of amorphous alumina which also broadens the 10 μm band towards the red. The optical constants of a-Al_20_3 are taken from Begemann et al. (1997).

In Fig. 6 the spectrum of EP Aqr is compared with a synthetic spectrum consisting of 48 vol.% $Ca_2Al_2SiO_7$, 23% Mg-Fe-ASG (x=3), 0.5% α-Al_2O_3, 20% a-Al_2O_3, and 8.5% $Fe_{0.4}Mg_{0.6}O$. The combination of the two ASGs reproduces the 10 μm band profile satisfactorily. The fit of the 13 μm band by spheres of α-Al_20_3 is not very good, but because shape effects play a significant role, it seems possible to reach a good fit by chosing an appropriate shape distribution (cf. Begemann et al. 1997) or by taking into account a heterogeneous grain structure (Kozasa & Sogawa 1997). The ASGs used for the modelling of the 10 μm band fail to reproduce the 20 μm band adequately. The missing absorption around 20 μm may be readily supplied by a MgFe oxide component (dashed line). The optical constants of this oxide were taken from Henning et al. (1995).

It is beyond the scope of this paper to provide an exact reproduction of the observed spectra. Here we only wished to illustrate that the variety observed among the infrared spectra of the circumstellar dust shells around evolved oxygen-rich stars may be evidence for mineralogical diversity. Currently, ISO provides spectra of improved quality and larger wavelength range compared to IRAS. For the interpretation of the ISO data, spectroscopic laboratory measurements reflecting this mineralogical diversity certainly will be required.

5. Summary and conclusions

Spectral data of more than 2000 oxygen-rich circumstellar envelopes which show silicate emission bands demonstrate considerable variety, especially in the 10 μm profile (Olnon & Raimond 1986). This fact implies that stardust silicates of a certain mineralogical diversity are present in the circumstellar dust shells. Thus, experimental work of laboratory astrophysics must cover a greater manifold of silicate dust analogues than the "canonical" amorphous Mg-Fe silicates. This paper is a first step towards such an extension.

1. Since there are clear indications that aluminium oxide is among the stardust components, Al is the first candidate on a list of elements to be taken into consideration, if the compositional range of the silicates is widened. Further candidates are calcium and sodium.
2. The overwhelming majority of the observed silicate spectra shows vibrational bands, the carriers of which must be strongly disordered or amorphous (vitreous) solids. The spectra of a number of evolved stars shows also clear evidence for the presence of crystalline silicates.
3. Considering items 1. and 2. and based on our experience with silicate glasses, several series of aluminosilicate glasses (ASGs) were synthesized, in which, apart from Mg and Fe, cations like Ca and Na have been admitted. In contrast to these cations, which act as modifiers of the glass network, in ASGs Al partially occupies the site of Si within the tetrahedra, i.e., Al acts together with Si as network former. The samples were thoroughly investigated by chemical and physical analytics.
4. For a total of 13 different ASGs, forming a sodium, a magnesium, a magnesium-iron (1:1 mixture), and a calcium series, optical constants have been determined in the wavelength range 6.7–500 μm. For the first time, for two of the samples n and k have been determined by scattering measurements of millimetre waves for the wavelengths from 2.73 to 4 mm. The calculated mass absorption coefficients at 4 mm for Rayleigh spheres of these ASGs amount to values of 0.1–0.2 cm^2g^{-1}.
5. For each ASG, the MIR spectrum for Rayleigh spheres has been calculated in order to derive diagnostic characteristics of these analogues. Tight correlations of the band positions, strengths, and widths with the SiO_2- and the Al_2O_3- contents of the samples have been established. They can be useful tools for future modelling of the circumstellar silicate spectra of evolved stars.
6. The IRAS LRS spectra of the Mira stars IK Tauri and EP Aqr have been used as examples for a simple demonstration of the potentials of the new analogues. Some of them have significantly larger opacity values in the trough region and flatter 20 μm profiles than the pyroxene and olivine glasses studied in Papers I and II.
7. It was demonstrated that an admixture of some percent of amorphous a-Al_2O_3 can effectively increase the trough absorption and, thus, remove the well-known trough opacity problem of silicate dust analogues. The representation of the 20 μm band can be improved by including Mg-Fe oxides as grain materials. We stress, however, that the fit of the observed spectra by special mixtures of analogues is ambiguous.
8. In combination with the hitherto existing silicate glasses the new analogues form a base for improved reproductions of the observed stardust spectra and more sophisticated envelope models.

Acknowledgements. The authors thank Gabriele Born, Jena, for her preparative and analytical work and Walter Teuschel, Jena, for the infrared measurements. We gratefully acknowledge the collaboration with H. Wagner, Professur Bauchemie der Bauhaus-Universität Weimar, in the chemical analysis. Further, we thank Elke Wagner, In-

stitut für Glaschemie der Friedrich-Schiller-Universität Jena for the X-ray diffractometry.

References

Begemann B., Dorschner J., Henning Th., et al., 1997, ApJ 476, 199
Bösch M.A., 1978, Phys. Rev. Letters 40, 879
Bradley J., Ireland T., 1996, in Physics, Chemistry, and Dynamics of Interplanetary Dust, eds. B. A. S. Gustafson and M. S. Hanner (San Francisco: ASP), p. 275
Dorschner J., Henning Th., 1986, Ap&SS 128, 47
Dorschner J., Begemann B., Henning Th., Jäger C., Mutschke H., 1995, A&A 300, 503 (Paper II)
Dorschner J., 1997, in Formation and Evolution of Solids in Space, ed. J. M. Greenberg (Dordrecht: Kluwer Acad. Publ.), in press
Gervais F., Blin A., Massiot D., et al., 1987, J. Non-Cryst. Solids 89, 384
Gürtler J., Henning Th., Dorschner J., 1989, Astron. Nachr. 310, 319
Gustafson B. Å. S., 1996, Journal of Quantitative Spectroscopy and Radiative Transfer 55, 663
Henning, Th., 1996, in The Cosmic Dust Connection, ed. J. M. Greenberg (Dordrecht: Kluwer Acad. Publ.), p. 399
Henning Th., Mutschke H., 1997, A&A 327, 743
Henning Th., Begemann B., Mutschke H., Dorschner J., 1995, A&AS 112, 143
Jäger C., Mutschke H., Begemann B., Dorschner J., Henning Th., 1994, A&A 292, 641 (Paper I)
Koike C., Hasegawa H., 1987, Ap&SS 134, 361
Koike C., Tsuchiyama A., 1991, in Origin and Evolution of Interplanetary Dust, ed. A. C. Levasseur-Regourd & H. Hasegawa (Dordrecht: Kluwer), p. 95
Koike C., Shibai H., Tsuchiyama A., 1993, MNRAS 264, 654
Kozasa T., Sogawa H., 1997, in ISOs View on Stellar Evolution, ed. R. Waters (Dordrecht: Kluwer Acad. Publ.), in press
Krätschmer W., 1988, in Experiments on Cosmic Dust Analogues, eds. E. Bussoletti, C. Fusco, & G. Longo (Dordrecht: Kluwer), p. 95
Lange J. 1991, in: Chemische Analyse glasiger Systeme, Deutscher Verlag für Grundstoffindustrie GmbH, Leipzig
MacPherson G. J., Wark D. A., Armstrong J. T., 1988, in Meteorites and the Early Solar System, eds. J. F. Kerridge and M. S. Matthews (Tucson: Univ. of Arizona Press), p. 746
McMillan P., 1984, Amer. Min. 69, 622
McMillan P., 1984, Amer. Min. 69, 645
Mysen B. O., Virgo D., Scarfe C. M., 1980, Am. Min. 65, 690
Mysen B. O., Virgo D., Kushiro I., 1981, Am. Min. 66, 678
Nuth III J. A., 1996, in The Cosmic Dust Connection, ed. J. M. Greenberg (Dordrecht: Kluwer Acad. Publ.), p. 205
Nuth III, J. A., Hecht, J. H., 1990, Ap&SS 163, 79
Olnon F. M., Raimond E., + IRAS Science Team, 1986, A&AS 65, 607
Palme H., Beer H., 1993, in: Landolt-Börnstein, New Series, Group VI, Vol. 3, Astronomy and Astrophysics, Extension and Supplement to Vol. 2, ed. H.H. Voigt, Springer Verlag, Berlin, p. 202
Sharma S. K., Virgo D., Mysen B. O., 1979, Am. Min. 64, 779
Sloan G. C., Price S. D., 1995, ApJ 451, 758
Stencel, R. E., Nuth III, J. A., Little-Marenin, I. R., Little, S. J., 1995, ApJ 350, L45
Tarte P., 1965, in Physics of Non-Crystalline Solids, ed. J.A. Prins (Amsterdam: North-Holland), p. 549
Waters L. B. F. M., Molster F. J., de Jong T., et al., 1996, A&A 315, L361
Whittet D. C. B., 1992, Dust in the Galactic Environment (Bristol: Institute of Physics Publishing)